

LATE CENOZOIC DISPLACEMENT TRANSFER ANALYSIS WITHIN  
DEEP SPRINGS VALLEY, EASTERN CALIFORNIA WITH GRAVITY MODELING

by

Sarah Anne Sokol



APPROVED BY SUPERVISORY COMMITTEE:

---

John F. Ferguson, Chair

---

John W. Geissman

---

Carlos L. V. Aiken

Copyright 2019

Sarah Anne Sokol

All Rights Reserved

Dedicated to Saul and Gladys Sokol, and Perry Leynor

LATE CENOZOIC DISPLACEMENT TRANSFER ANALYSIS WITHIN DEEP SPRINGS  
VALLEY, EASTERN CALIFORNIA WITH GRAVITY MODELING

by

SARAH ANNE SOKOL, BS

THESIS

Presented to the Faculty of  
The University of Texas at Dallas  
in Partial Fulfillment  
of the Requirements  
for the Degree of

MASTER OF SCIENCE IN  
GEOSCIENCES

THE UNIVERSITY OF TEXAS AT DALLAS

May 2019

## ACKNOWLEDGMENTS

I would like to thank my advisors and committee members, John Ferguson, John Geissman, and Carlos Aiken, for their support in this endeavor. Their aid and expertise was integral to the completion of this research. In addition, I thank John Oldow for his assistance in the field and for laying the foundation on which this research was built.

My appreciation for the support and assistance I received from other University of Texas at Dallas students cannot be understated. I thank Nicholas Mueller and August Ridde for assisting in the collection of data for this research and for their continued support following the field season.

Apart from all others, I thank Lauren Landreneau whose partnership is invaluable and whose assistance and encouragement was an immeasurable source of fortitude.

I thank The University of Texas at Dallas Department of Geosciences for their support and confidence in the pursuit of this research.

This work was supported by Pioneer Natural Resources and The University of Texas at Dallas.

December 2018

LATE CENOZOIC DISPLACEMENT TRANSFER ANALYSIS WITHIN DEEP SPRINGS  
VALLEY, EASTERN CALIFORNIA WITH GRAVITY MODELING

Sarah Anne Sokol, MS  
The University of Texas at Dallas, 2019

Supervising Professor: John F. Ferguson

The northern segment of the Eastern California Shear Zone (ECSZ) is characterized by right-lateral transtension accommodated on a network of north-northwest and northwest striking dextral transcurrent faults connected by north-northeast striking normal faults. North-northeast faults bounding Deep Springs Valley, California, transfer displacement from the Owens Valley-White Mountain fault system in eastern California eastward to the Fish Lake Valley (FLV) fault. The FLV fault is the northern segment of the most active structure in the ECSZ and marks the eastern boundary of the zone of right-transtensional displacement east of the Sierra Nevada. Deep Springs Valley is 22 km long and 5 km wide and is bounded by a prominent north-northeast striking fault on the southeast that, to the northeast, emanates into six east-northeast splays transferring displacement east. The northwest boundary of the basin is marked by a more subdued north-northeast trending fault zone stretching the length of the basin. 381 gravity stations at a nominal 300 m spacing were collected as part of a gravity survey within the basin. The residual gravity data shows a -13.2 mGal gravity low in the southeastern part of the basin that gradually increases to -4.7 mGal to the northeast. The residual gravity values correspond to

depths of about 0.85 and 0.2 km, respectively. Restoration to a pre-extensional datum, using an extension direction of N65W, yields a cumulative horizontal extension of ~1930 m across the basin fault system, which corresponds to an equal amount of right lateral displacement transferred to the FLV fault system. The estimated extension rate of 0.58 mm/yr since 4 Ma or 1.1 mm/yr if displacement was initiated at 1.7 Ma.

## TABLE OF CONTENTS

ACKNOWLEDGMENTS.....	v
ABSTRACT.....	vi
LIST OF FIGURES.....	ix
CHAPTER 1 INTRODUCTION.....	1
CHAPTER 2 REGIONAL TECTONIC FRAMEWORK.....	4
CHAPTER 3 STRUCTURE AND STRATIGEPAHY OF DEEP SPRINGS VALLEY .....	7
3.1 Physiography .....	7
3.2 Structural Geology.....	8
3.3 Stratigraphy .....	9
CHAPTER 4 SUBSURFACE BASIN MORPHOLOGY .....	12
4.1 Gravity Methods .....	12
4.2 Subsurface Morphology .....	14
4.3 2D Forward Models.....	16
CHAPTER 5 FAULT MODEL AND DISPLACEMENT BUDGET.....	21
5.1 Fault Model .....	21
5.2 Displacement Component Determination and Displacement Budget .....	22
CHAPTER 6 DISCUSSION AND CONCLUSION .....	28
APPENDIX FIGURES.....	31
REFERENCES.....	44
BIOGRAPHICAL SKETCH.....	48
CURRICULUM VITAE.....	49



## LIST OF FIGURES

Figure A.1	Regional physiographic map of the northern Eastern California Shear Zone.....	31
Figure A.2	Physiographic map of Deep Springs Valley.....	32
Figure A.3	Simplified geologic map of Deep Springs Valley .....	33
Figure A.4	Acquired gravity stations in Deep Springs Valley surrounding environs.....	34
Figure A.5	Complete Bouguer Anomaly map of the northern Eastern California Shear Zone...35	
Figure A.6	Complete Bouguer Anomaly map for Deep Springs Valley.....	36
Figure A.7	Residual Complete Bouguer Anomaly map of Deep Springs Valley.....	37
Figure A.8	Map of Deep Springs Valley for cross section reference.....	39
Figure A.9	Two-dimensional models.....	40
Figure A.10	Displacement budget for Deep Springs Valley.....	43

## CHAPTER 1

### INTRODUCTION

Assessment of an integrated displacement budget in a diffuse zone of intracontinental deformation is made difficult by the complexity of the fault geometry and how that complexity allows displacement to be transferred among different fault segments that comprise the fault system. In a diffuse zone of deformation, comprised of a pattern of strike-slip and dip-slip faults, faults typically behave as a system of integrated structures (Burchfiel et al., 1987; Burchfiel and Stewart, 1966). Kinematic links between faults have been established on regional and single fault scales where displacement is transferred and accommodated through the interaction of multiple faults and fault segments (Oldow, 1992; Stewart, 1988; Burchfiel et al., 1987; Burchfiel and Stewart, 1966; Renik and Christie-Blick, 2015). The interaction of faults, and variation in shear sense and orientation within systems of faults results in varying magnitudes of displacement along strike (Reheis and Dixon, 1996; Frankel et al., 2007, 2011a). Significant variation in the magnitude of displacement in a fault system can be attributed to the distribution of displacement on other segments and strands of a fault or through the transfer of displacement out of the system by related structures (Reheis and Dixon, 1996; Frankel et al., 2007, 2011a).

The Eastern California Shear zone is a transtension-dominated zone of deformation in which an array of strike-slip and dip-slip faults are kinematically and temporally related. Dextral displacement in the ECSZ is distributed across a series of subparallel, northwest-striking strike-slip fault zones and displacement transfer between those zones is accommodated by northeast trending normal faults (Oldow, 1992; Reheis and Dixon, 1996; Stewart, 1988; Lee et al., 2001). The right-lateral faults in the ECSZ have fault traces up ~300 km long and are separated by ~20-

30 km. The normal faults that kinematically link the major strike-slip fault zones often produce extensional basins that accommodate displacement transfer. The interaction between the strike-slip and dip-slip faults of the ECSZ results in variation of the magnitude of displacement along fault segments (Reheis and Dixon, 1996; Renik and Christie-Blick, 2015; Frankel et al., 2011b). This variation in displacement magnitude is observed on the major dextral fault systems of the ECSZ by up to a factor of three along strike (Frankel et al., 2011b) and is attributed to displacement transfer and distribution of displacement on multiple fault segments (Reheis and Dixon, 1996; Frankel et al., 2011b).

In the northern ECSZ, most right-lateral displacement is localized on the Fish Lake Valley fault zone (Bennet et al., 2003; Dixon et al., 2000; Frankel et al., 2011; Reheis and Dixon, 1996). Displacement decreases from south to north by ~30 km (Mckee, 1968; Renik and Christie-Blick, 2013), which is attributed to WNW-trending left-oblique faults that accommodated displacement and transfer displacement to the east. Several of these transfer fault systems have been assessed to account for the decrease of displacement on the Fish Lake Valley fault zone. However, in order to calculate a comprehensive displacement budget for the Fish Lake Valley fault zone, displacement transferred in to the system must also be evaluated.

The Deep Springs Valley fault zone (DVSFZ) is a northeast trending transfer fault between two of the strike-slip master faults in the ECSZ, the Owens Valley and Fish Lake Valley fault zones (Reheis and Dixon, 1996; Lee et al., 2001). The DSVFZ (Figure A.1) is dip-slip dominated and bounds the east side of Deep Springs Valley, a 25-km long pull-apart basin (Lee et al., 2001). The DSVFZ displays a decrease in vertical displacement by a factor of two over a 10 km distance (Lee et al., 2001). Although the origin of variation in the magnitude of

displacement on faults has been studied regionally in the ECSZ, the origin of similar displacement variation on smaller faults in this system has not been explored.

This study evaluates the method and magnitude of transfer within Deep Springs Valley fault system and on to the Fish Lake Valley fault zone, using gravity modelling. A fault model of the Deep Springs Valley fault zone and associated faults was produced to explore potential origins in displacement variation along strike in smaller transfer zones and to quantify the displacement contribution to the regional displacement budget. In addition, the structural model that results from this study provides a comprehensive examination of the local displacement budget.

## CHAPTER 2

### REGIONAL TECTONIC FRAMEWORK

The Eastern California Shear Zone (ECSZ) and Central Walker Lane are regions of right-lateral transtension that accommodate differential motion between the Sierra Nevada block and the Basin and Range Province and together accounts for about 25% of the total relative motion between the Pacific and North American plates (Argus and Gordon, 1991; Dixon et al., 2000; Oldow, 2003; Bennett et al., 2003). Transtensional deformation in the region began at about 4 Ma (Oldow et al., 2008) and an extension direction of N65W is well documented from 4 Ma to present using fault slip inversion, recorded seismicity and contemporary GPS velocities (Oldow, 2003). In the northern ECSZ (Figure A.1), displacement is distributed across the Owens Valley-White Mountain (OV-WM), Hunter Mountain- Panamint Valley (HMPV), and Death Valley-Furnace Creek-Fish Lake Valley (DV-FC-FLV) fault zones (Frankel et al., 2011b). The characteristic faults of the ECSZ are NW-trending, right-oblique faults and are connected by a series of NE-trending normal faults which behave as right steps, transferring displacement northeast (Reheis and Dixon, 1996; Burchfiel et al., 1987). Displacement from the HM-PV fault zone is transferred to the DV-FC-FLV fault zone via the NE-trending dip-slip faults that opened Saline and Eureka Valley, isolating displacement in far northern ECSZ on to the OV-WM and FLV fault zones (Dixon et al., 1995; Dixon et al., 2000; Reheis and Dixon, 1996).

Geodetic modeling and fault displacement determinations suggest that up to 90 percent of right-oblique displacement in the northern ECSZ occurs on the FLV fault zone (Bennet et al., 2003; Dixon et al., 2000; Frankel et al., 2011; Reheis and Dixon, 1996). Although 10-20% of displacement also occurs on the OV-WM fault zone, estimates show a wide range of 15 to 65%

of displacement from the OV-WM fault zone is transferred to the DV-FC-FLV fault zone on the DSVFZ, north of the termination of the HM-PV fault zone (Figure A.1) (Reheis and Dixon, 1996; Lee et al., 2001).

Variations in displacement along strike in the ECSZ of a factor of two or more have been reported on the DV-FC-FLV and OV-WM fault zones over distances as short as ~30 km (Kirby et al., 2008; Frankel et al., 2007, 2011b; Ganey et al., 2010). The Fish Lake Valley fault zone experiences a loss of 30 km of right lateral displacement from south to north. Southern Fish Lake Valley has a total lateral offset of ~50 km based on apparent offset of the Beer Creek Pluton (Mckee, 1968; Renik and Christie-Blick, 2013) yet northern Fish Lake Valley has ~20 km of displacement based on an apparent offset of a thrust fault of Paleozoic age (Renik and Christie-Blick, 2013). The variation in the magnitude of displacement is attributed to distributed faulting occurring between the major dextral systems, commonly resulting in extension (Renik and Christie-Blick, 2015; Reheis and Dixon, 1996; Frankel et al., 2011b; Oldow, 1992). West-northwest striking left-oblique faults transfer displacement off the FLVFZ to the east. Similarly, there is a loss of displacement by more than a factor of two along the Owens Valley-White Mountain fault zone. Contemporary slip rates along this fault zone decrease from 1.2 mm/yr in the south to >0.5 mm/yr in the north. This variation in displacement is not exclusive to the primary dextral faults in the ECSZ. Such variations in magnitude are also observed along strike of faults that kinematically link the primary faults and transfer displacement between them.

The Deep Springs Valley fault zone is part of an extensional transfer system that formed Deep Springs Valley (DSV) and has been shown to have vertical displacement variation along

strike by a factor of two over a 10 km distance, and temporal variations by a factor of 4.5 over the course of millions of years (Lee et al., 2001). Detailed geologic mapping has been done in this region and previous studies have provided slip rates on the DSVFZ. The Deep Springs Valley fault zone bounds the eastern side of Deep Springs Valley (Figure A.1, Figure A.2) which is bounded to the west by antithetic normal faults. Deep Springs Valley and its associated fault zone intersect FLV to the northeast via east-northeast trending normal faults and two northeast-striking left-lateral faults (Lee et. al., 2001). The DSVFZ intersects the far northern part of the OVFZ, where the OVFZ joins the WMFZ, to the southwest by way of NE-striking normal faults that connect the southern tip of Deep Springs Valley through the southern range to OV (Reheis and Dixon, 1996). Precambrian and Cambrian meta-sedimentary rocks, and Jurassic to Cretaceous aged monzonites underlie the southern and northern halves of the valley, respectively. Overlying the range north of the basin is a sequence of Cenozoic sandstone, tuff and a basalt flows dated at 11.6 Ma (Mueller, 2018). Slip rates vary spatially and temporally along the DSVFZ and slip rates calculated by Lee et al. (2001) place the onset of deformation for the DSVFZ at 1.7 Ma, which demonstrates that Deep Springs Valley formed under the contemporary extension direction, N65W. Although structural analysis of the DSVFZ by Lee et. al. (2001) demonstrates that DSV is a right step, normal-fault system that has a southwest to northeast decrease in the magnitude of displacement, a mechanism for displacement variation and the amount of displacement transferred has not been assessed in detail.

## CHAPTER 3

### STRUCTURE AND STRATIGRAPHY OF DEEP SPRINGS VALLEY

#### Section 3.1: Physiography

Deep Springs Valley is an elongated, northeast-trending basin (Figure A.2) that separates the Inyo and White mountains to the southeast and northwest, respectively. Deep Springs Valley is 24-km long and varies in width from north to south from 3 km to 9 km, respectively. The eastern margin of the basin is primarily a linear feature, whereas the western margin has a western extending arm. The closed nature of the basin has resulted in a playa lake, known as Deep Springs Lake, in the south of the basin. The basin elevation ranges from 1700 m in the north to its lowest elevation of 1500 m in the south, at Deep Springs Lake.

Deep Springs Valley is completely surrounded by highlands and mountain ranges. The range to the east of DSV, here after referred to as the Deep Springs Ridge (DSR), is a part of the Inyo Mountain range and separates DSV from Eureka Valley. The Deep Springs Range is ~4 km wide and reaches its highest elevation of 2350 m at Chocolate Mountain, previously known as Piper Peak, which is located 2 km from the northeast corner of DSV. The basin contact with the DSR is sharp and steep. DSV is separated from Fish Lake Valley, to the north, by 6 km of highlands that reach elevations of up to 2100 m. West of DSV are the White Mountains, a northwest trending range that extends for 65 km. Locally, the elevation of the White Mountains ranges between 1800 m and 2400 m. This western margin of DSV has a shallower, gradational elevation change, especially to the southwest, relative to the eastern margin. DSV is separated from Owens Valley, to the south, by 6.5 km of highlands with a maximum elevation of 2600 m.



All the highlands surrounding Deep Springs Valley are predominantly composed of Jurassic and Cretaceous plutonic rocks, and Paleozoic and Precambrian meta-sedimentary rocks.

### **Section 3.2: Structural Geology**

Deep Springs Valley (Figure A.2) is predominantly bounded to the east and west by north-northeast striking normal faults. The most substantial structure is the Deep Springs Valley fault zone, which is a 26-km long north-northeast striking, normal fault. Previous studies have established that the DSVFZ is the primary source of displacement in Deep Springs Valley (Lee et al., 2001; Reheis and Sawyer, 1996). Although its average orientation is N23E (Lee et al., 2001), the northern part of the DSVFZ is distinct in that its orientation progressively changes to the north-northwest with a south-southeastern dip direction. The DSVFZ consists of multiple parallel strands, with scarps that suggest the faults become progressively younger toward the interior of the basin (Lee et al., 2001).

The Deep Springs Range contains a broad, dispersed zone of NNE-trending normal faults whose extent follows the length of the range and borders western Eureka Valley. In the vicinity of Soldier Pass the traces of faults in the range become progressively more ENE to E-W oriented to the north. These faults are presumed to have NNW to north dips and become progressively more sinistral as their orientations shift towards E-W, based on the regional extension direction. The southern region of Deep Springs Valley consists mainly of north-northeast trending faults in the range and bounding the basin. The triangle shaped morphology of southern DSV is due to the convergence of the bounding faults, where the western basin bounding fault trends north and the eastern basin bounding fault, the DSVFZ, turns northeast.

Western Deep Springs Valley consists of both antithetic and synthetic, normal faults with varying vertical offsets. The fault traces are expressed in the southern and northern sides of the western basin, but most disappear into basin sediment cover in central DSV. These faults are potentially long continuous features that stretch the length of the basin. The northern extent of these western faults begins to bifurcate and splay, producing a wider zone of faulting with varying orientations.

Faults north of Deep Springs Valley differ from the rest of the system, presumably due to their roles in displacement transfer to the Fish Lake Valley fault zone. The northeast corner of the range has a series of east-northeast to east-west trending left oblique faults, most of which contact the DSVFZ at the basin margin. This cluster of left-oblique faults is bound by two left lateral faults to the north and south, and serves as the basis of displacement transfer between the Deep Springs Valley fault system and the Fish Lake Valley fault zone (Reheis and Sawyer, 1997).

### **Section 3.3: Stratigraphy**

The Inyo and White Mountain ranges that flank Deep Springs Valley to the southeast and northwest, respectively, are locally composed of Precambrian and Paleozoic meta-sedimentary rocks, Jurassic and Cretaceous aged monzonite intrusions, and Cenozoic sequences of sandstone, tuff, and basalt (Figure A.3). Deep Springs Valley is distinctly split, by a north-northwest contact that separates the Precambrian and Paleozoic meta-sedimentary rocks to the southwest and the Jurassic and Cretaceous intrusions to the northeast. Younger volcanic and sedimentary rocks exclusively appear north of DSV, nonconformably on top of Jurassic plutonic rocks.

Precambrian and Paleozoic meta-sedimentary rocks are exposed outside the south and southwestern side of the basin in both the Inyo and White Mountain ranges. These carbonate and siliciclastic meta-sedimentary rocks have undergone significant deformation and have a total thickness of over 6.5 km (Nelson, 1978). Heavily faulted and folded, these rocks have shallow to moderate dips, although the dips steepen to 60° - 80° when in close proximity to the plutons to the northeast (Miller, 1928). Jurassic monzonites exposed in the northern half of Deep Springs Valley vary in composition from the quartz monzonite of Beer Creek to the hornblende-augite monzonite of Joshua Flat. Cretaceous aged granite dikes and small masses are found along the Precambrian-Paleozoic and Beer Creek contact, northwest of DSV. North of DSV, a sequence of tuffaceous sandstone, rhyolitic tuff, and basalt dated, at 11.6 Ma (Mueller, 2018), found directly on plutonic rocks and are in contact with valley sediments. The Cenozoic tuff and basalt lie on Chocolate Mountain, outside the northeastern corner of the valley at an elevation of ~2350 meters.

Most of the valley is covered in sandy, poorly consolidated Quaternary alluvium and alluvial fan deposits that grade into silt and clay approaching Deep Springs Lake. Dating of Quaternary deposits in the eastern part of DSV show that alluvial fan deposits are as young as early Holocene age and some debris flows have been documented to be less than ~480 years old (Lee et al., 2001). An isolated sedimentary section of sandstone, tuff, and tephra is also found east of DSV, north of Soldier Pass at the edge of the valley, in contact with valley sediments and along faults in the Deep Springs Ridge. Lee et al. (2001) dated three units within the section, which placed deposition between mid-Miocene and mid-Pleistocene time. The sedimentary section is found exposed in the hanging wall and footwall of the DSVFZ (Lee et al, 2001) and

therefore can be used to evaluate slip rates on the DSVFZ. The sequence contains a basal conglomerate dated at 15.1 +/- 0.1 Ma and a distinct pumiceous tuff marker horizon, 140 m above the base, dated at 3.09 +/- 0.08 Ma (Lee et. al, 2001). The tephra exposed at the top of the section has been identified as a deposit of the Bishop Ash with an  $^{40}\text{Ar}/^{39}\text{Ar}$  age of 756 +/- 34 ka was established (Lee et. al, 2001).

## CHAPTER 4

### SUBSURFACE BASIN MORPHOLOGY

#### Section 4.1: Gravity Methods

To ascertain and evaluate the subsurface structures of Deep Springs Valley a detailed relative gravity survey was conducted. 2D forward models were produced through the reduction of collected and publically acquired absolute gravity measurements to residual complete Bouguer anomalies. Basin depths were constrained in the north and south-southcentral regions of the basin by a well that extends to the basement and by previous seismic studies, respectively.

381 gravity stations were collected during this study along accessible roads and two west-northwest oriented, cross-country transects (Figure A.4). The location of gravity stations was controlled, primarily, by the density of sage brush and by the quality of the roads, with the exception of the two transects collected on foot. Gravity measurements were taken using two Scintrex CG-5 Autograv gravimeters at a spacing of 300 m. Three meter readings were taken at each station. Each reading consisted of 60 seconds of gravity sensor data. Each occupation value is an average of the three gravity readings. The relative gravity measurements were tied to a base station located at an NGS monument in Fish Lake Valley. The gravity base station in Fish Lake Valley is tied to an absolute gravity station, National Geodetic Survey Gravity Reference Base Station 0455-1, located at the Tonopah airport 8 miles east of Tonopah, Nevada.

Station positioning for each gravity station was provided by two Leica Viva dual frequency Global Navigation Satellite System (GNSS) units in Real Time Kinematic mode. Rover receivers were tied to a GNSS base station receiver, located centrally in the basin. The base station was located relative to the Continuous Observation Reference System (CORS)

Network using the National Geodetic Survey supported website Online Positioning User Service (OPUS). Subsequent post processing of relative GNSS positions to the OPUS corrected base station was done using Leica GeoOffice. The base station is located at 37° 20' 39.33859375", 118° 1' 35.19811125" at an elevation of 1523.0319 m, +/- 0.01525 m.

Gravity data from this study were reduced to the complete Bouguer anomaly (CBA) (Figure A.5). Collected stations were terrain corrected using a MatLab program, gravproc, developed by John Ferguson at The University of Texas at Dallas. The inner (Cogbill, 1989) and outer (Plouff, 1966) terrain corrections utilized 1/3 arc-second, 10 m DEM data and 1 arc-second, 30 m DEM data, respectively, acquired from The National Map developed by the United States Geological Survey's (USGS) National Geospatial Program. Terrain corrections were done in accordance to the standards set by the USGS (Hildebrand et al., 2002). Gravity data from this study was merged with 3,561 stations taken by other University of Texas at Dallas students between 2012 and 2016 and stations from the Pan American Center for Earth Sciences (PACES), totaling to over 80,000 gravity stations over a 194,000 km<sup>2</sup> area. 32 PACES stations are located within and in close proximity to DSV. A Bouguer anomaly was calculated using the Holom and Oldow (2007) spreadsheet, employing a reduction density of 2.67 g/cm<sup>3</sup>. The Bouguer anomaly values were gridded at 300 m spacing using a minimum curvature cubic spline algorithm in Oasis Montaj Geosoft.

A residual anomaly (Figure A.7) was calculated using the Mickus et. al. (1991) technique that eliminates the regional gravity trend and attempts to separate the gravity anomaly produced by the basin fill. The regional gravity field was calculated using the same method for calculating a CBA but only includes stations, collected by PACES and other UTD studies, outside the basin

margin. The regional gravity field is then subtracted from the Bouguer gravity and the residual gravity signal represents the gravitational effect due to the basin fill and local geologic structures.

#### **Section 4.2: Subsurface Morphology**

Analysis of the Bouguer gravity and residual anomalies for Deep Springs Valley and the surrounding region can reveal large magnitude structures and density contrasts. First order analysis of the Bouguer gravity at a regional scale (Figure A.5) shows a relatively flat gradient, which becomes less negative from northwest to southeast. Large scale gravity lows appear over Owens Valley and Fish Lake Valley with gravity trends oriented along strike of the major basin bounding faults. There is circular gravity low in the White Mountains, ~7 km east of Deep Springs Valley, that is controlled by a signal data point and is likely an artifact of interpolation caused by lack of sufficient data coverage. Locally, relative regional gravity highs are confined to a north-northwest trending gravity high follows the length of the Last Chance Range connected to a less linear high over southern Eureka Valley and the Saline Range. In the vicinity of Deep Springs Valley, the gravity gradient runs parallel to the long axis of the basin. Northeast trending gradients over Deep Springs Ridge appear to be a function of eastern Deep Springs Valley, in conjunction with northwestern Eureka Valley. The Bouguer gravity gradient within Deep Springs Valley (Figure A.6) is significantly steeper to the east and shallower to west, which corresponds to the relatively large magnitude Deep Springs Valley fault zone that bounds the eastern margin of the basin and indicates Deep Springs Valley is an asymmetric basin. Following the long axis of the basin, to the northeast, the Bouguer gravity trending becomes

progressively more symmetrical. Two localized, circular gravity lows appear in the south and north of the basin, with maximum low Bouguer gravity values of -220.9 mGal and -210.8 mGal, respectively. These localized gravity lows indicate that Deep Springs Valley is segmented in to two sub-basins, of which the southern sub-basin contains a deeper basin fill to bedrock contact. Far southern and southwestern DSV have the highest Bouguer gravity values, which suggests that basin depth in these regions is relatively shallow and potentially superficial.

The residual anomaly (Figure A.7), in conjunction with local geologic context, provides a more detailed examination of gravitational perturbations confined to Deep Springs Valley. The gradients in the residual anomaly closely mirror large scale gradient characteristics in the Bouguer gravity, indicating that the residual anomaly is an acceptable approximation of the gravity signature restrained to the basin. The residual anomaly has a maximum low value of -13.2 mGal located at Deep Springs Lake in the south of basin that decreases gradationally in a northeasterly orientation at a rate of 0.9 mGal/km until a -4.7 mGal low in northern Deep Springs Valley that is separated by a -2.2 mGal high. The gravity gradients between the maximum gravity low and the western and eastern margins of the basin are 3.1 mGal/km and 6 mGal/km, respectively. The residual anomaly does not fully extend to the southern and southwestern margins of the basin, implying that the basin sediment in these areas is superficial, akin to a pediment style sediment contact. This observation is similarly reflected in the Bouguer anomaly. The eastern margin of the basin does not contain many stations on bedrock and so this margin is poorly constrained. Where there is sufficient data, the residual anomaly shows a steeper gradient to the east, relative to the western margin, with local gravity lows hugging the eastern margin, which coincides with the Deep Springs Valley fault zone. Two small gravity lows appear



centrally in the basin. The -9.0 and -8.0 mGal lows coincide with stations at their locations, however, there is no data coverage between them. These lows can be interpreted as small, localized areas of increased depth, or as a continuous, gradational feature that is not accurately expressed in the residual anomaly due to lack of data. The residual anomaly has a bottleneck feature in the vicinity of Deep Springs College, where the gravity lows are less significant and the gradient is much shallower than the rest of the basin. This implies a loss of depth, and therefore a potential loss of displacement within the basin fault system.

### **Section 4.3: 2D Forward Models**

#### ***Methods and Limitations***

To assess basin geometry and displacement partitioning in Deep Springs Valley, two-dimensional forward models were produced along collected gravity transects (Figure A.8). The 2D models constrain the locations and orientations of subsurface structures, and allow for a quantitative evaluation of displacement along structures. Geologic maps, previous seismic studies and well data were used as constraints and initial input data for 2D model production. An iterative process was employed to match the calculated residual anomaly values based on geologic models to the observed residual anomaly values, until minimal error and structural compatibility across transects was obtained. A cross section aligned with the basin axis, that crosses all other transects, was constructed to test the internal consistency of the 2D models and fault model.

Despite constraints, two-dimensional gravity modeling has several limitations. Off-axis bodies perturb accurate determinations of depth. In areas where this issue was recognized, 2.75D

modeling was utilized to alleviate error. Locations and orientations of subsurface structures are constrained by geologic maps and the gravity gradient along each transect. Typically, steep gradients represent substantial faults and shallow gradients can be reproduced with a series of smaller faults or ramps. Due to data spacing of 300 m, structures smaller than this threshold cannot be precisely detected. Moderate to major faults can be located in the gravity gradient but precise determinations of dip angles were only applied to large structures in which the gravity gradient provided adequate guidance. Locations of smaller structures were determined by inflection of the gravity gradient and were assigned 60° dips. Apparent dips were used in cases where the cross sections cross the faults obliquely. For larger structures, the Deep Springs Valley fault zone in particular, faults dips were determined using the gravity gradient. At this resolution, series of closely spaced, minor faults are likely to be represented as one moderately sized structure.

Constant densities were applied to the geologic units included in the 2D models (Table A.1). Precambrian and Paleozoic meta-sedimentary rocks were assigned an average density of 2.7 g/cm<sup>3</sup>. These rocks are undifferentiated due to the vast quantity and variety of the 11 local formations, and the complexity of pre-Miocene faulting and folding. The structural and lithologic heterogeneity of these rocks makes differentiation of these units untenable. Geophysical studies conducted by Pakiser et al. (1964) in the region utilized a density of 2.7 g/cm<sup>3</sup> for this undifferentiated sequence based on lithologic studies done by Anderson (1937) who observed extreme metamorphism imposed on the sedimentary rocks of the White and Inyo mountains, and density measurements obtained from samples in the region. Jurassic and Cretaceous plutonic rocks were assigned a density of 2.67 g/cm<sup>3</sup>. This density value reflects the traditional value for

crystalline granitic rocks (Hinze, 2003). A  $2.2 \text{ g/cm}^3$  was assigned to the valley fill based on studies done by Pakiser et al. (1964), who used this density after seismic refraction studies and comparison to seismic and gravity studies done by Shell Oil Co. The average contrast density between Cenozoic and Pre-Tertiary rocks calculated in other studies is  $-0.4$  or  $-0.5 \text{ g/cm}^3$  (Kane et al., 1960) and was employed in our models as well. The upper 53 meters of valley fill was assigned a density of  $2.0 \text{ g/cm}^3$  to represent unsaturated valley fill. Depth of this layer is determined by the water table, which was measured at 53 meters in a well north of Deep Springs College.

### *Description of 2D Models*

#### Transect A

Transect A (Figure A.9a) lies in the most northern region of the basin. This transect is not a straight feature and bends approximately halfway through its extent. The western segment of this transect is oriented north-northwest and the eastern segment is oriented northwest. The gravity gradient along this transect is relatively shallow with a maximum low anomaly of  $-3.36 \text{ mGal}$  that corresponds with the maximum basin depth of  $\sim 192 \text{ m}$ . The DSVFZ bounds the eastern margin of this transect and has a dip of  $35^\circ$ . The eastern-most dip slips faults strike north-northwest to north-northeast. The western margin is represented by a series of antithetic normal faults. These are north-northeast to north striking faults. With the exception of the DSVFZ, all faults were modelled using a  $60^\circ$  dip, although apparent dips were employed in the models as necessary. The overall error on Transect A is  $0.089 \text{ mGal}$ .

### Transect B

Transect B (Figure A.9b) crosses the basin in a west-northwest orientation and is situated centrally in Deep Springs Valley, ~1.7 km south of Soldier Pass. The gravity gradient to the west is moderate and contains an undulation across an outcrop of bedrock. Following the undulation, to the east, the gradient steepens and is represented by eastern facing, dip slip faults. The eastern margin of the basin has a steep, western facing gravity gradient that is represented by three strands of the DSVFZ that dip 40°. The center of the basin contains a modest left-oblique fault. The maximum gravity low in this transect is -8.1 mGal and corresponds to the maximum basin depth of ~505 m for this transect. The overall error on Transect B is 0.198 mGal.

### Transect C

Transect C (Figure A.9c) is orientated west-northwest and is located in the south-central region of Deep Springs Valley. This transect stretches across the widest extent of the basin, including the western arm. The gravity gradient on the far western side is relatively flat and signifies that basin sediment cover in this area is superficial. Towards the center of this transect, the gravity gradient steepens. Faults, antithetic to the DSVFZ, produce a step style basin geometry. The western side of the gradient is relatively steep and corresponds to the DSVFZ. The DSVFZ in this transect is represented by two faults strands with 45° dips. The center of the basin is a flat horizon that tilts to the east, towards the DSVFZ. The maximum gravity low is ~9.0 mGal. Although the lowest anomaly corresponds with a depth of ~495 m, the maximum basin depth along this transect is ~540 m due to the tilting of the central basin block. The overall error on Transect C is 0.188 mGal.

## Transect D

Transect D (Figure A.9d) crosses the southern end of the basin, oriented roughly east-west, along the northern side of Deep Springs Lake. The gravity gradient along this transect is steepest on the eastern side and is significantly more shallow on the western third. The far western side of Transect D is represented by eastern facing dip-slip faults with modest offset. As the gravity gradient becomes steeper to the east, the antithetic faults progressively produce more offset. The eastern gradient is represented by three strands of the DSVFZ with a  $60^\circ$  dip to the west. The maximum gravity low of -13.2 corresponds to a basin depth of 835 m. The maximum basin depth along this transect is ~850 m. The overall error on Transect D is 0.238 mGal.

## CHAPTER 5

### FAULT MODEL AND DISPLACEMENT BUDGET

#### 5.1: Fault Model

The Bouguer gravity, residual gravity anomaly, 2D models, and local and regional geologic maps were used to produce a fault model for Deep Springs Valley. Gradients in the residual anomaly constrained the subsurface basin morphology and exposed the locations and orientations of major structures buried under valley sediments. The 2D forward models provided a more detailed examination of the location and orientation of structures within the basin. Lateral continuity of structures was determined by the analysis of the 2D models and study of local geologic maps. Geologic maps also provided context to fault behavior in the system and provided locations of faults entering and exiting the basin.

Deep Springs Valley is an elongated, extensional basin. The orientation of the basin axis and faults are predominantly perpendicular to sub-perpendicular to the established extension direction of N65W. The basin is bounded by synthetic and antithetic normal faults that produce a basin geometry similar to that of a half-graben. A first order analysis of local geologic maps clearly delineates the fault system geometry and behavior changes at a boundary marked by Soldier Pass.

South of Soldier Pass, the basin geometry presents as a simple half-graben produced by synthetic and antithetic normal faults. The eastern margin sector is bounded by a west dipping, normal fault zone, the DSVFZ, which presents as a series of parallel strands whose strike is N23E on average. The dip of the Deep Springs Valley fault zone varies from 40° to 60°, from north to south, respectively. The rate of change in dip in this sector varies from 5.8 °/km, north

of Deep Springs Lake, to  $1.7 \text{ }^\circ/\text{km}$ , just south of Soldier Pass. The DSVFZ is the primary control on basin depth and the thickest sections of valley fill are in its vicinity. The western margin is characterized by a wide and dense zone of antithetic, normal faults. The western most faults are linear features that are parallel to the DSVFZ. The inner antithetic faults have orientations that change along strike from N to NNE. Four of these western faults extend across the full length of basin. Just south of Soldier Pass, a N65E striking, left-oblique fault cuts across the basin. Several antithetic faults terminate at their intersection with this fault and this fault cuts the DSVFZ.

North of Soldier Pass, the DSVFZ fragments in to several strands that vary in orientation. In general, the orientation of each strand progressively turns from NNE to NNW. The behavior of the Deep Springs Valley fault zone becomes progressively more oblique as the orientation changes. The dip of the basin-bounding strand of the DSVFZ decreases to  $35^\circ$  in northern Deep Springs Valley. The western margin in this sector contains antithetic, NNE-trending dip-slip faults that originate in the south of the basin. The western normal faults converge with NNW trending normal faults in the northwestern corner of the basin. The change in fault dip and behavior in this sector generates a shallower and more symmetric shaped basin than what is observed in the southern sector.

## **5.2: Displacement Component Determination and Displacement Budget**

To quantitatively estimate the horizontal extension in the Deep Springs Valley fault system, offset was measured on individual faults along four transects. The transects are orientated parallel to sub-parallel to the regional extension direction, N65W. An additional transect that lies on the basin axis was constructed to tie the WNW oriented transects together and provided an

additional method of auditing the validity of the fault model. Vertical offsets on structures were determined from 2D geologic models, based on residual gravity anomalies, and geologic maps and cross sections. Cumulative offset along each transect was calculated to test the fault model for this system and to determine the total displacement transferred to the Fish Lake Valley fault zone from the Deep Springs Valley fault system.

### ***Displacement Component Determination***

The horizontal extension along a fault is the horizontal component of the net-slip, which during regional extension is oriented in the extension direction. The nature of the geophysical model does not permit direct measurement of the net slip along a structure, however, vertical offset derived from 2D models, and fault orientations provide necessary inputs for calculating the components of net slip.

The vertical component of net-slip, vertical off-set, is calculated by restoring fault blocks to an elevation of an established pre-deformation depositional surface. In the case of the Deep Springs Valley fault system, faults were restored to an elevation of 2350 m, based on a contact between the erosional surface of a monzonite intrusion and a Tertiary basalt flow dated at 10.8 Ma (Mueller, 2018). This contact is located on top of Chocolate Mountain, located northeast of Deep Springs Valley. Restoration to a pre-extension datum was done along each modelled transect, where the current depth of fault blocks is derived. Although, it is probable that clusters of small faults are represented as single larger structures in the 2D models, the vertical offsets on these faults should have minimal error and adequately represent the aggregate vertical offset.



The strikes and dips of faults were estimated using geologic maps, residual anomaly gradients and the proposed fault model. Some fault strikes were measured directly off geologic maps. For faults buried under basin sediments, estimations were made with heavy consideration of the geologic context. Normal faults, that lacked other relevant information, were assigned dips of 60°. Fault dips were measured from geologic cross sections. For some faults with substantial offsets or considerably different geometry from the rest of the system, dips were determined through modeling faults to fit the gradient of the residual anomaly. Any faults represented with their apparent dips in the 2D models are calculated with respect to their true dips.

The horizontal extension and net slip were calculated for each structure using the estimated vertical offset, true dip, and strike, in conjunction with the regional extension direction, N65W. The first step to calculate the horizontal extension is to project the vertical component of displacement to a horizontal plane, normal to the strike of the fault.

$$D_{HC} = \frac{V}{\tan(\theta)}$$

V = Vertical component of displacement

$\theta$  = Dip angle of fault

The  $D_{HC}$  is then projected on to the azimuth of the extension direction. This is calculated using the  $D_{HC}$  and the acute angle between the strike of the fault and the regional extension direction, N65W.

$$HE = D_{HC} / \sin \varphi$$

$D_{HC}$  = Dip slip projected the horizontal plane, normal to the strike of the fault

$\varphi$  = Acute angle between the fault strike and extension direction

The net-slip on each structure was calculated using the estimated vertical offset and horizontal extension. This calculation is done with the assumption that all slip is parallel to the extension direction.

$$NS = \sqrt{V^2 + HE^2}$$

V = Vertical component of displacement

HE = Horizontal extension component

### ***Displacement Budget***

The purpose of determining a displacement budget across the Deep Springs Valley system is twofold; a displacement budget tests the model for internal consistency and ultimately, produces a quantifiable assessment of displacement transfer within and by way of the fault system (Fig 5.1). To produce a displacement budget, the horizontal extension and net slip is calculated for each structure at the intersection of the fault and the transect. If the fault model is geometrically possible, the horizontal extension and net-slip along each transect should be the same.

Discrepancies in total displacement between transects implies that the blocks experience internal deformation, the fault model is not feasible, or that the fault system is not closed and that displacement is being transferred to other structures outside the scope of the proposed fault model.

The location of 2D models, in which aggregate horizontal extension is calculated, was solely determined by the distribution and orientation of gravity stations within the valley. In an ideal study, all modeled transects would be oriented parallel to the regional extension direction. Due to the density of sage brush and road access, or lack thereof, the transects modeled for this study are each oriented approximately north-northwest, with the exception of the most northern

transect, Transect A. Although the bulk of structures considered in this system are measured in the 2D models, faults within the range that contribute to the displacement within the system are also included in the displacement budget. Orientations and displacement estimations for these faults are obtained from geologic maps and cross sections. In cases where there is no cross section to estimate the displacement along a fault in a certain locale, DEM data was used on erosional surfaces to estimate minimum vertical offset. Cumulative horizontal extension was calculated along each transect (Figure A.10).

The southern transect crosses the deepest part of Deep Springs Valley. The Deep Springs Valley fault zone contributes 961 m of horizontal extension and accounts for 1922 m of net-slip. The additional 972 m of horizontal extension is distributed across antithetic and synthetic dip slip faults, west of the Deep Springs Valley fault zone. Cumulative horizontal extension and net slip along this transect is 1962 m and 3896 m, respectively.

The south-central transect crosses the widest section of Deep Springs Valley. The Deep Springs Valley fault zone in this area accounts for 1394 m of horizontal extension and 1970 m of net slip. Cumulative horizontal extension and net slip along this transect is 1897 m and 2951 m, respectively.

The north-central transect accounts for 1986 m of cumulative horizontal extension and 3000 m of cumulative net slip. The Deep Springs Valley fault zone contributes 1475 m of horizontal extension and 2001 m of net slip. This transect crosses a left-oblique fault that cuts the DSVFZ and accounts for 59 m of horizontal extension and 97 m of net slip.

The northern transect crosses the northern sub-basin and has a cumulative horizontal extension and net slip of 1876 m and 2834 m, respectively. The Deep Springs Valley fault zone has a total horizontal extension of 1339 m and net slip of 1592 m.

## CHAPTER 6

### DISCUSSION AND CONCLUSION

The Deep Springs Valley fault system produces an extensional basin that transfers displacement from the Owens Valley-White Mountain fault zone to the Fish Lake Valley fault zone.

Quantitative assessment of the magnitude of displacement transferred via the basin fault system results in ~1930 m of displacement. This ~1930 m value represents the horizontal extension across the basin and corresponds to the fault system's contribution of lateral displacement on the Fish Lake Valley fault zone. The horizontal extension values taken from four transects across the basin have a maximum percent difference of 5.7%, which suggests a geometrically plausible model. Although horizontal extension is maintained throughout the basin, net slip decreases significantly from south to north along the basin axis, with a maximum percent difference of 31.6%.

The Deep Springs Valley fault zone contributes 50% or more of net slip along each transect, and therefore is the primary singular source of displacement within the system. The DSVFZ varies in dip from north to south from 35° to 60°, respectively. Despite the considerable decrease in vertical offset and net-slip to the north, horizontal extension is maintained throughout the system. The increase in dip to the south, in conjunction with the increase of vertical offset allows for the preservation of horizontal extension while significantly increasing net-slip.

Displacement transfer from the Owens Valley-White Mountain fault zone to the Fish Lake Valley fault zone via the Deep Springs Valley fault system yields additional discrepancies to the overall Fish Lake Valley fault zone displacement budget. Assuming the onset of contemporary extension, starting at 4 Ma, is concurrent with the onset of basin formation the

Deep Springs Valley system contributes  $\sim 0.5$  mm/yr of slip to the FLVFZ. This slip rate is compatible with the south to north  $>0.7$  mm/yr loss of slip along the OV-WM fault zone but is not consistent with slip rates along the FLVFZ. Displacement transfer on to the FLVFZ should result in an increase of slip north of the intersection of the DSV fault system but instead a decrease in slip is observed on the FLV fault zone. Loss of displacement along the Fish Lake Valley fault zone is well documented and research pertaining to the cause is on-going (Frankel et al., 2007; Frankel et al., 2007; Mckee, 1968; Renik and Cristie-Blick, 2013). Present studies demonstrate that 3 mm/yr of slip is lost between Cucomongo Canyon and Furnace Creek, and additional 0.6 mm/yr of slip is lost between Furnace Creek and Indian Creek, based on minimum slip rates (Frankel et al., 2011b). In addressing this issue, previous and ongoing studies have attributed 9-10 km of displacement loss on the Fish Lake Valley fault zone due to displacement transfer on to structures east of Fish Lake Valley (Dunn et al., 2015; Katapody, 2018; Mueller, 2018). Although this study makes no effort to alleviate displacement discrepancies on the Fish Lake Valley fault zone, it does demonstrate that the magnitude of displacement loss along the fault zone is potentially larger than the present values, even if current minimum slip rates underestimate displacement on the Fish Lake Valley fault zone.

Results from this study are congruent with previously established knowledge of Deep Springs Valley. Wilson (1975) determined a basin depth of 792 m using seismic refraction and gravity modeling along Transect D from this study. This is a 5% difference between Wilson's value and the maximum basin depth value derived from this study, 835 m. Lee et al. (2001) estimated that 15-65% of displacement on the Owens Valley fault zone to transferred out of the system along the Deep Springs Valley fault zone. Using an average contemporary slip rate for

the Deep Springs Valley system determined in this study, and Pleistocene slip rates on the OVFZ, approximately 40% of displacement on the OVFZ is transferred to FLV via the DSV fault system. Lee et al. (2001) also provides an estimation for the onset of deformation along the DSVFZ based on offsets of the Bishop Ash, dated at 756 +/- 34 ka, and a tuff marker bed dated at 3.09 +/- 0.08 Ma. Lee et al. (2001) estimates the onset of deformation along the Deep Springs Valley fault zone began at 1.7 Ma and that the horizontal extension rate along the fault is 0.7 mm/yr. Using the minimum and maximum horizontal extension values along the Deep Springs Valley fault zone determined in this study and an onset date of 1.7 Ma, horizontal slip rate on the DSVFZ ranges from 0.56 mm/yr to 0.86 mm/yr, which closely brackets the 0.7 mm/yr estimation made by Lee et al. (2001).

Although significant variability of horizontal extension along the Deep Springs Valley fault zone has been observed, up to 39% difference, horizontal extension is maintained across the entirety of the system. The Deep Springs Valley fault zone is the primary single contributor to displacement within the basin fault system and accounts for as much as ~75% of total horizontal extension in some parts of the basin. Based off horizontal extension values from this study, the average horizontal slip rate for the Deep Springs Valley fault system ranges between 0.5 mm/yr and 1.1 mm/yr, using the onset of contemporary extension and onset of basin formation according to Lee et al. (2001) as bounding times.

## APPENDIX

### FIGURES

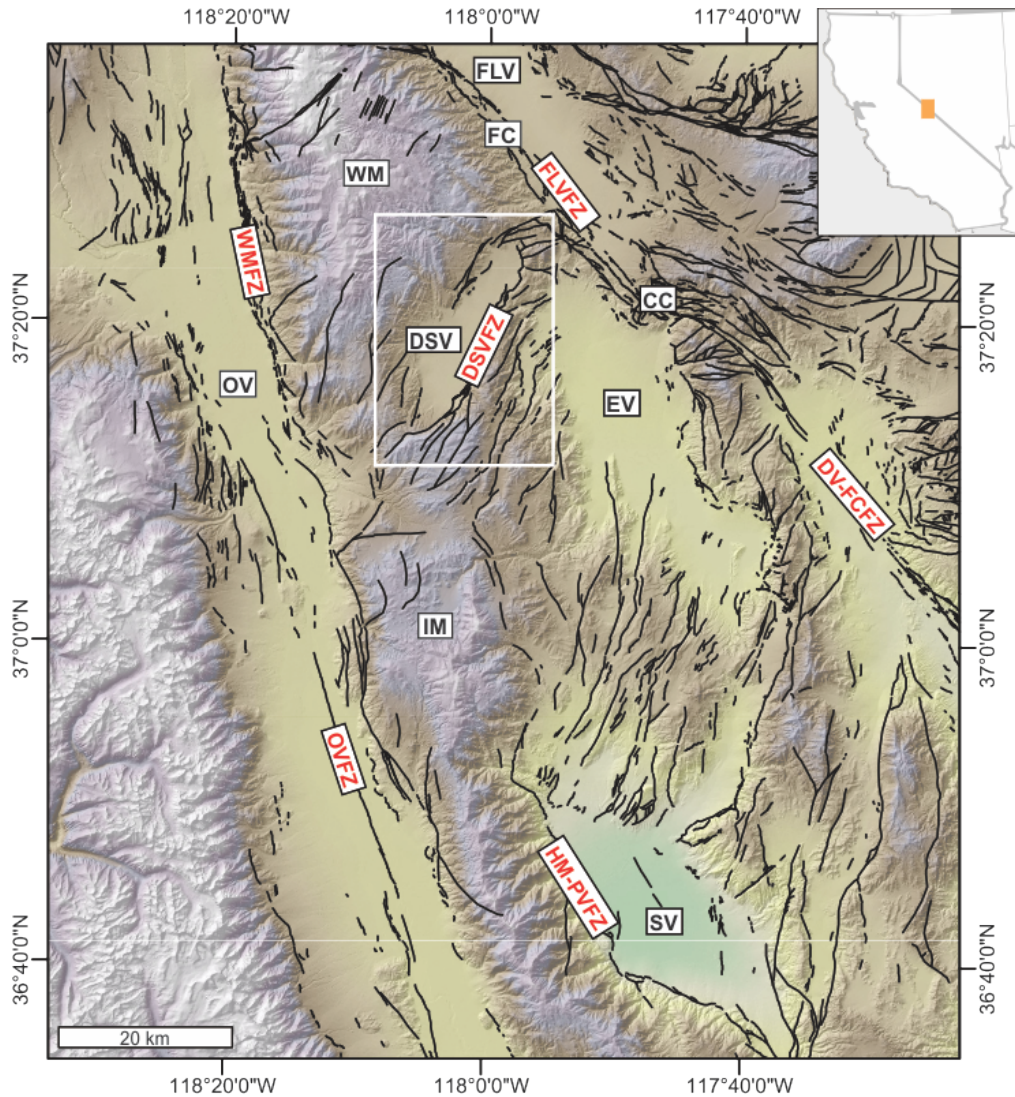


Figure A.1: Shaded relief map of the northern Eastern California Shear Zone, displaying fault traces in black. Physiographic locations are labeled in black and major fault systems are labeled in red. CC – Cucomongo Canyon, DV-FCFZ – Death Valley-Furnace Creek Fault Zone, DSV – Deep Springs Valley, DSVFZ – Deep Springs Valley Fault Zone, EV – Eureka Valley, FLV – Fish Lake Valley, FLVZ – Fish Lake Valley Fault Zone, FC – Furnace Creek, HM-PVFZ – Hunter Mountain-Panamint Valley Fault Zone, OV – Owens Valley, OVFZ – Owens Valley Fault Zone, SV – Saline Valley, WMFZ – White Mountain Fault Zone.



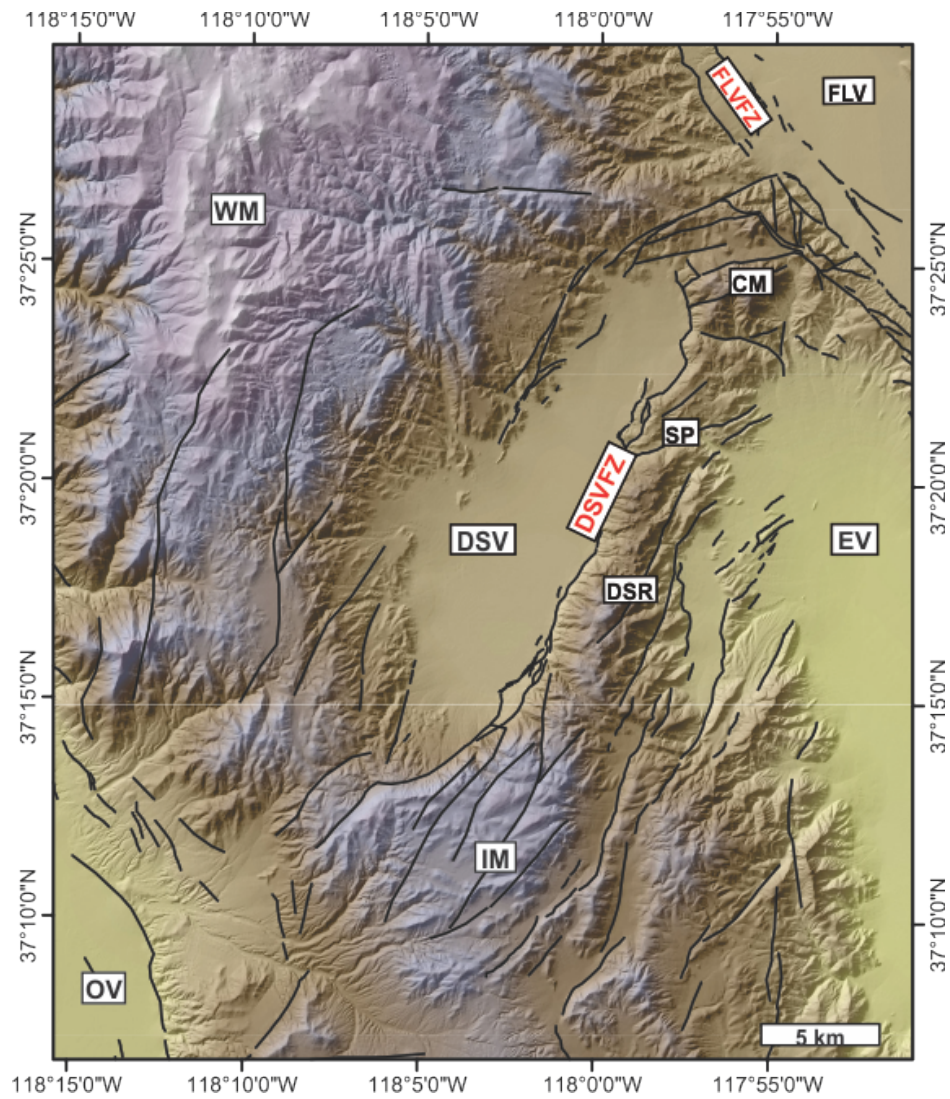


Figure A.2: Physiographic map of Deep Springs Valley and local environs with fault traces in black. CM – Chocolate mountain, DSR – Deep Springs Ridge, DSV – Deep Springs Valley, EV – Eureka Valley, FLV – Fish Lake Valley, FLVFZ – Fish Lake Valley fault zone, IM – Inyo Mountains, OV – Owens Valley, SP – Soldier Pass, and WM – White Mountains.

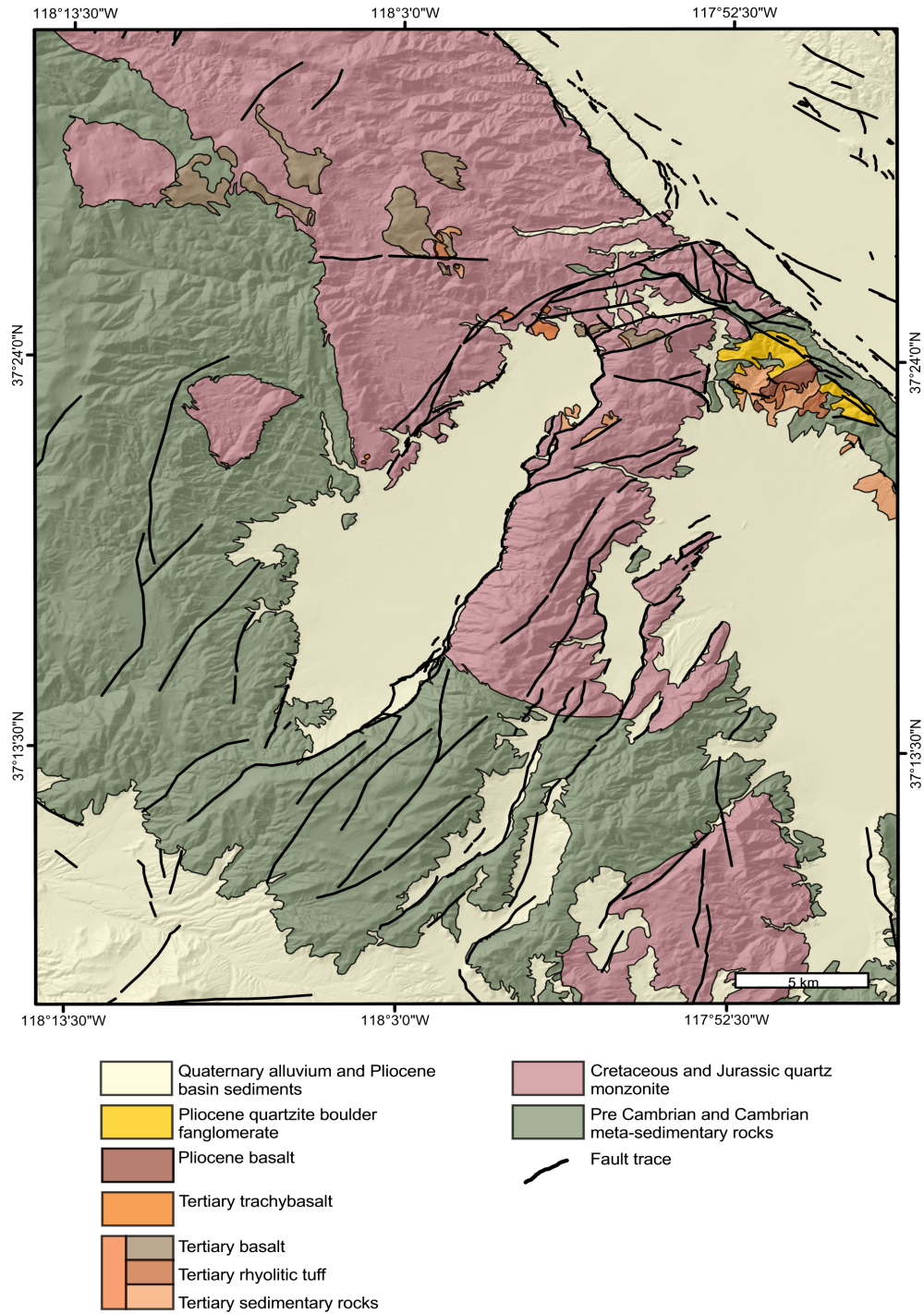


Figure A.3: Simplified geologic map of Deep Springs Valley modified from Nelson, 1966, Nelson, 1971 and, Mckee and Nelson, 1967. Fault traces are shown in black.

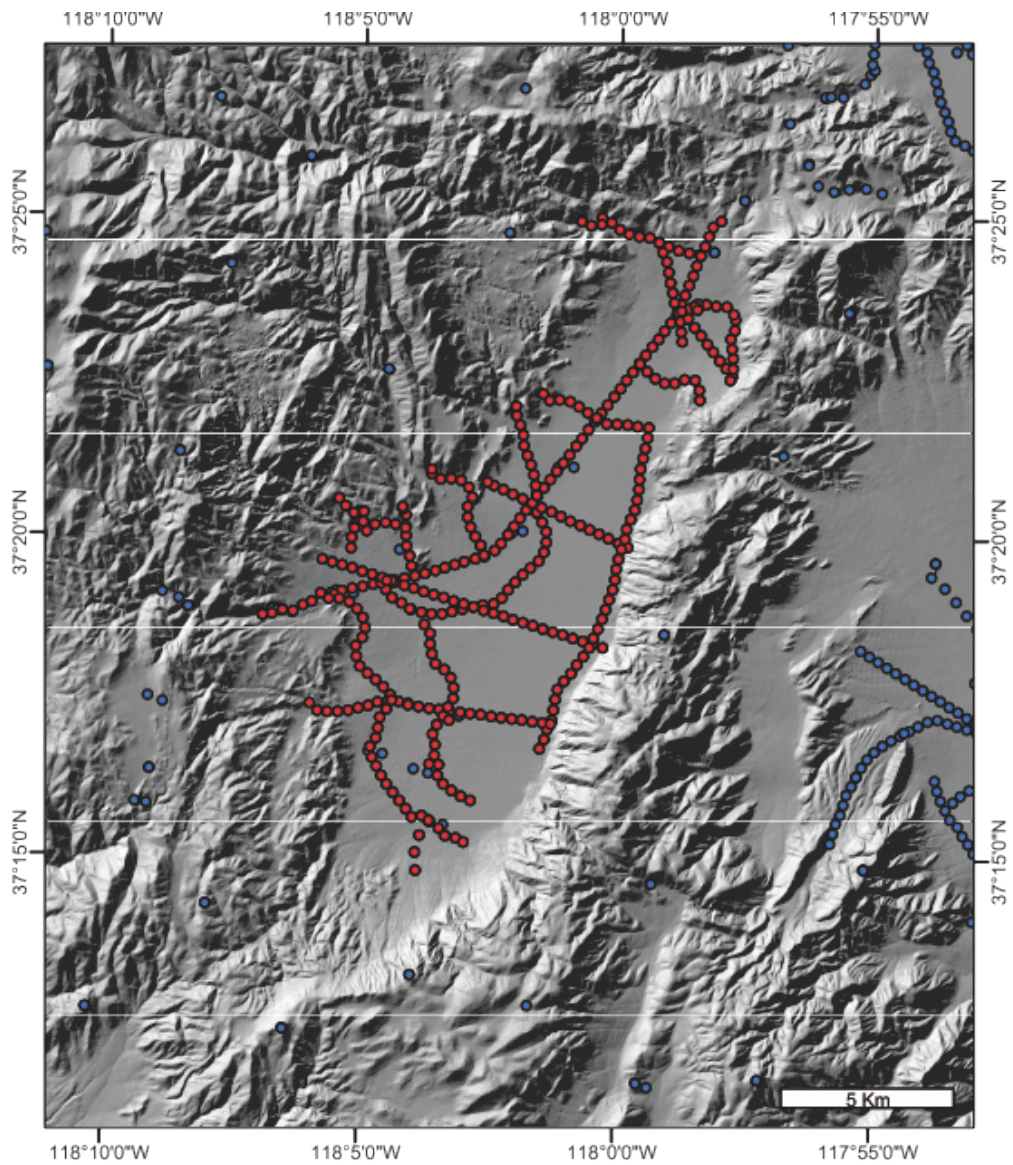


Figure A.4: Gravity survey map showing 381 gravity stations collected for this study (red) and merged with stations previously gathered by The University of Texas at Dallas and provided by the Pan American Center for Earth Sciences (blue) within 5 km of Deep Springs Valley.

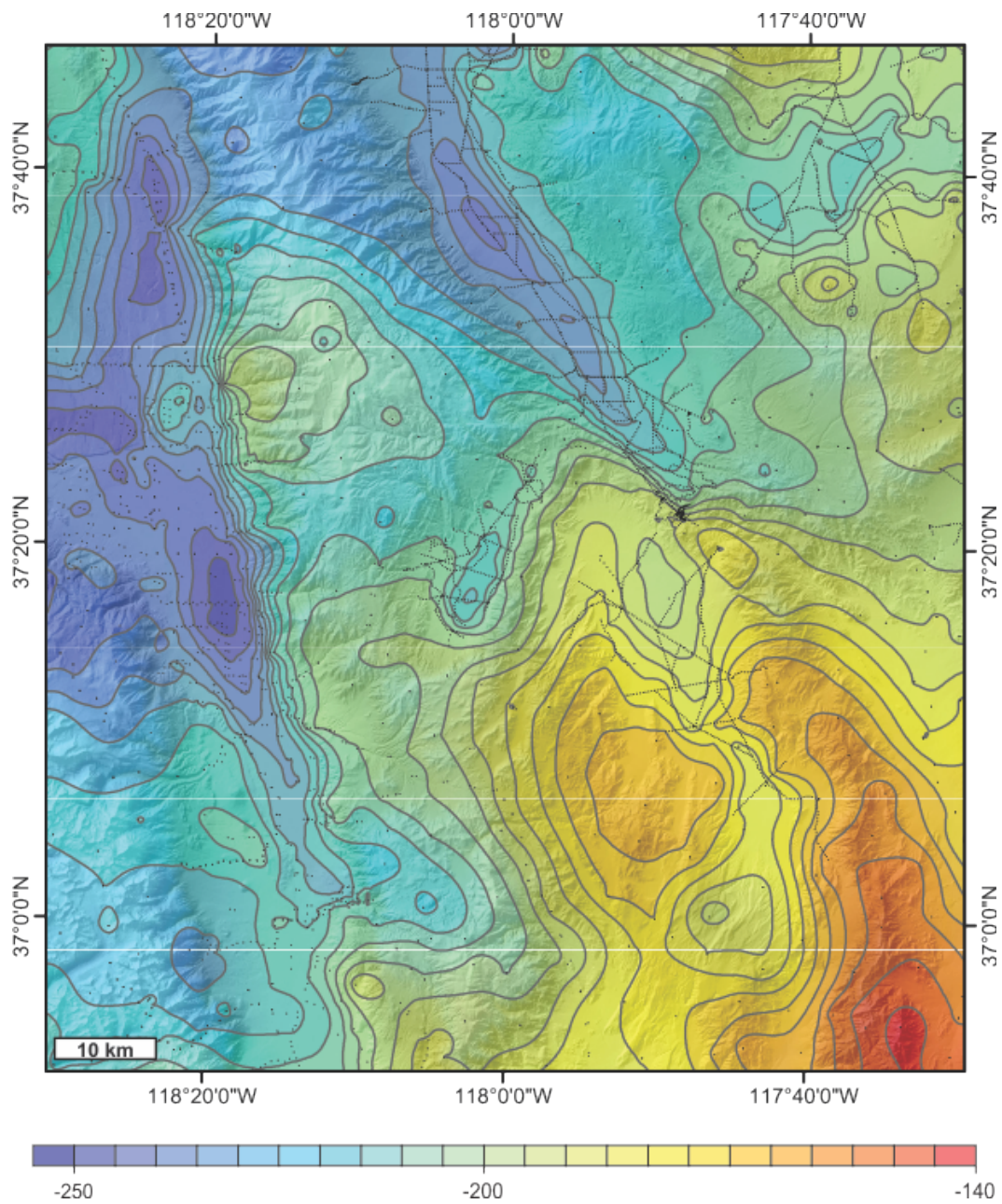


Figure A.5: Bouguer gravity map of the northern Eastern California Shear Zone with 5 mGal contours in grey and station locations in black. Deep Springs Valley lies within the center of the figure.

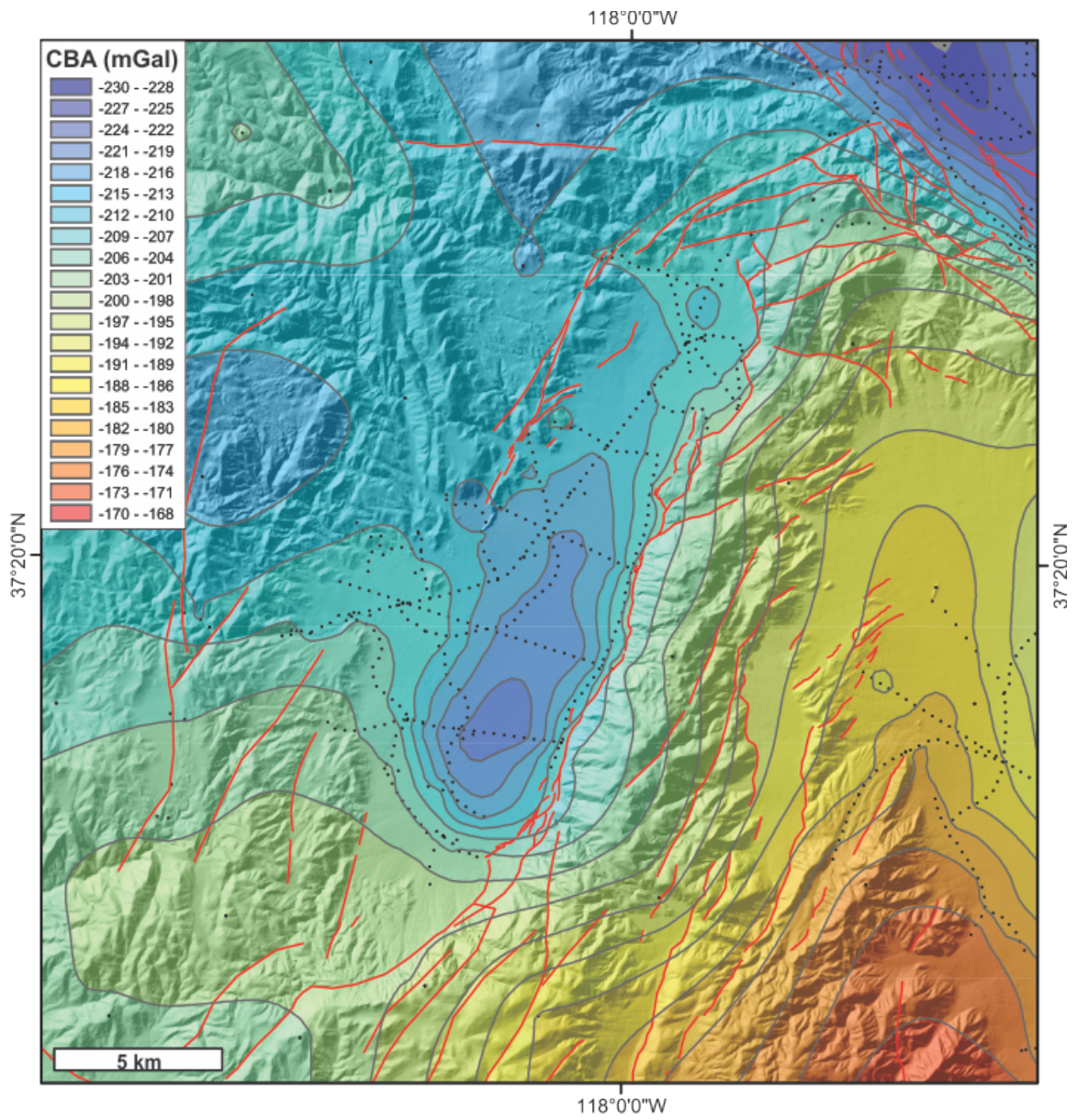


Figure A.6: Bouguer gravity map of Deep Springs Valley and local environs with 3 mGal contours in grey, station locations in black, and fault traces in red.

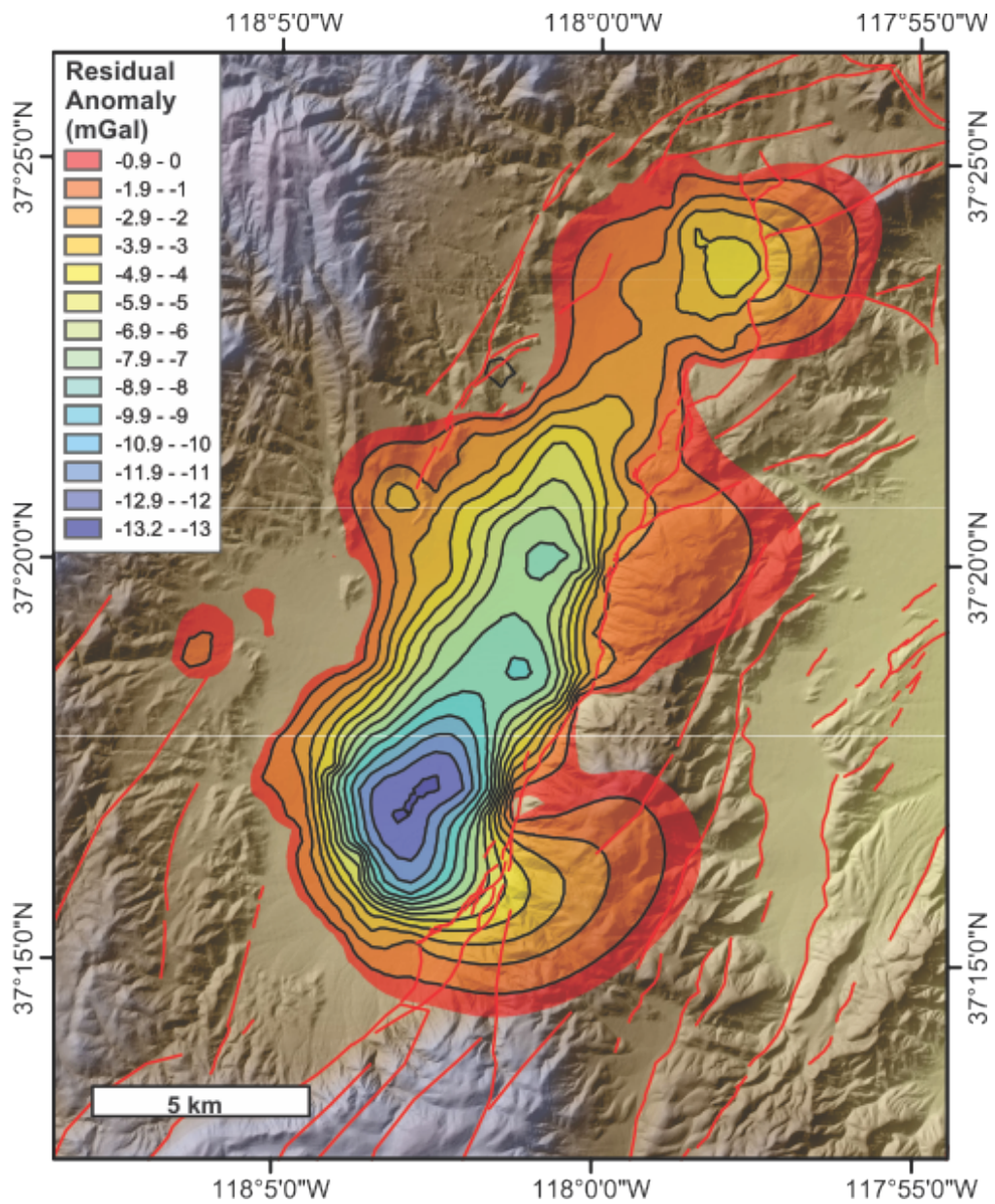


Figure A.7: Residual anomaly map of Deep Springs Valley and local environs with 1 mGal contours in black and fault traces in red.

Table A.1: Lithologic descriptions and densities for two-dimensional forward models.

Unit	Description	Density (g/cm <sup>3</sup> )
Qal	Unsaturated sediments, upper 53 m	2.0
	Quaternary alluvium and alluvial fan deposits	2.2
Tb	Tertiary basalt, dated at 10.8 Ma	2.9
Tv	Tertiary rhyolitic tuff and sandstone, undifferentiated	2.4
Jg	Jurassic monzonites, including Quartz monzonite of Beer Creek and Hornblende-augite monzonite of Joshua Flat	2.67
Pz	Pre-Cambrian and Paleozoic meta-sedimentary rocks, undifferentiated	2.7

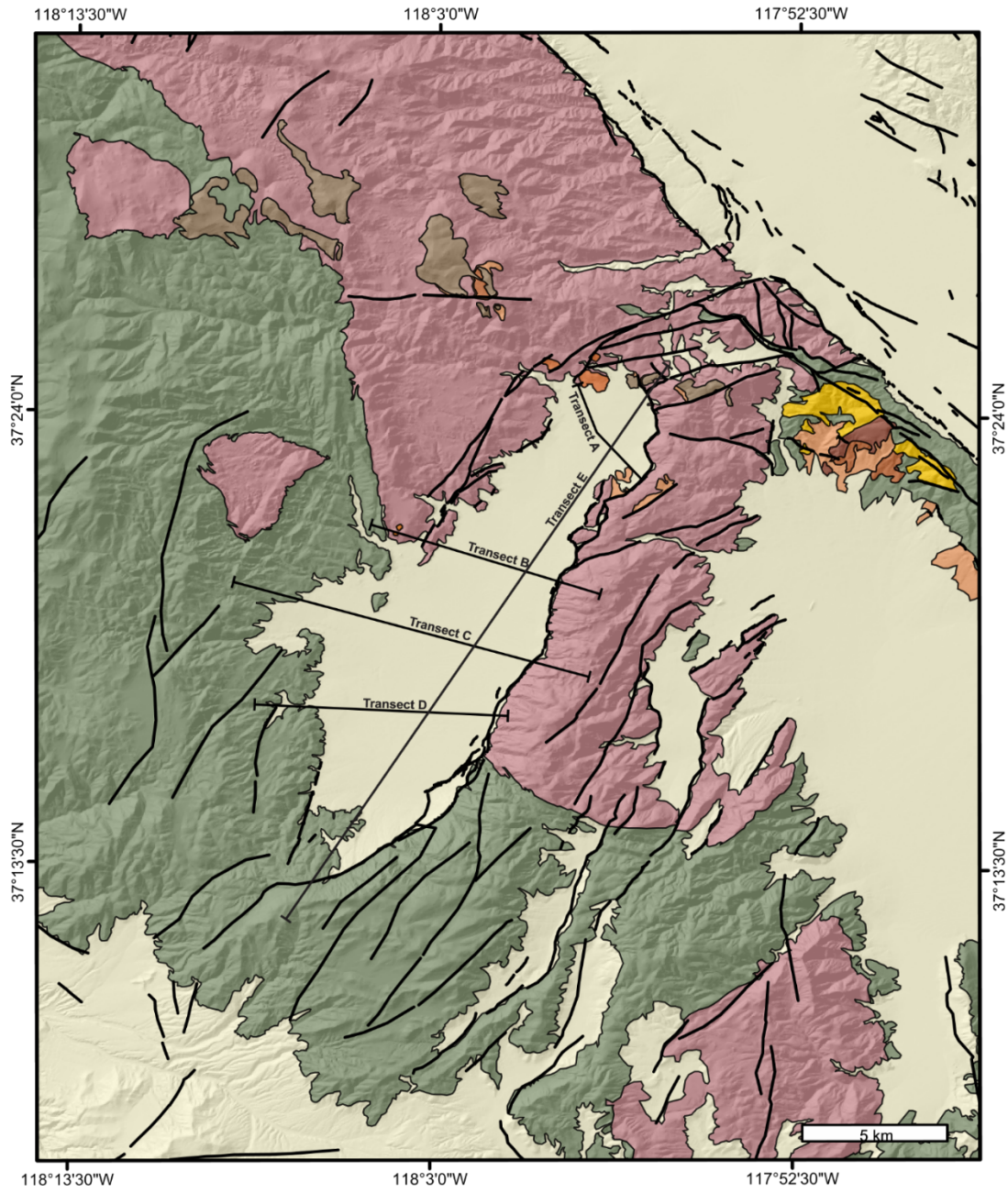
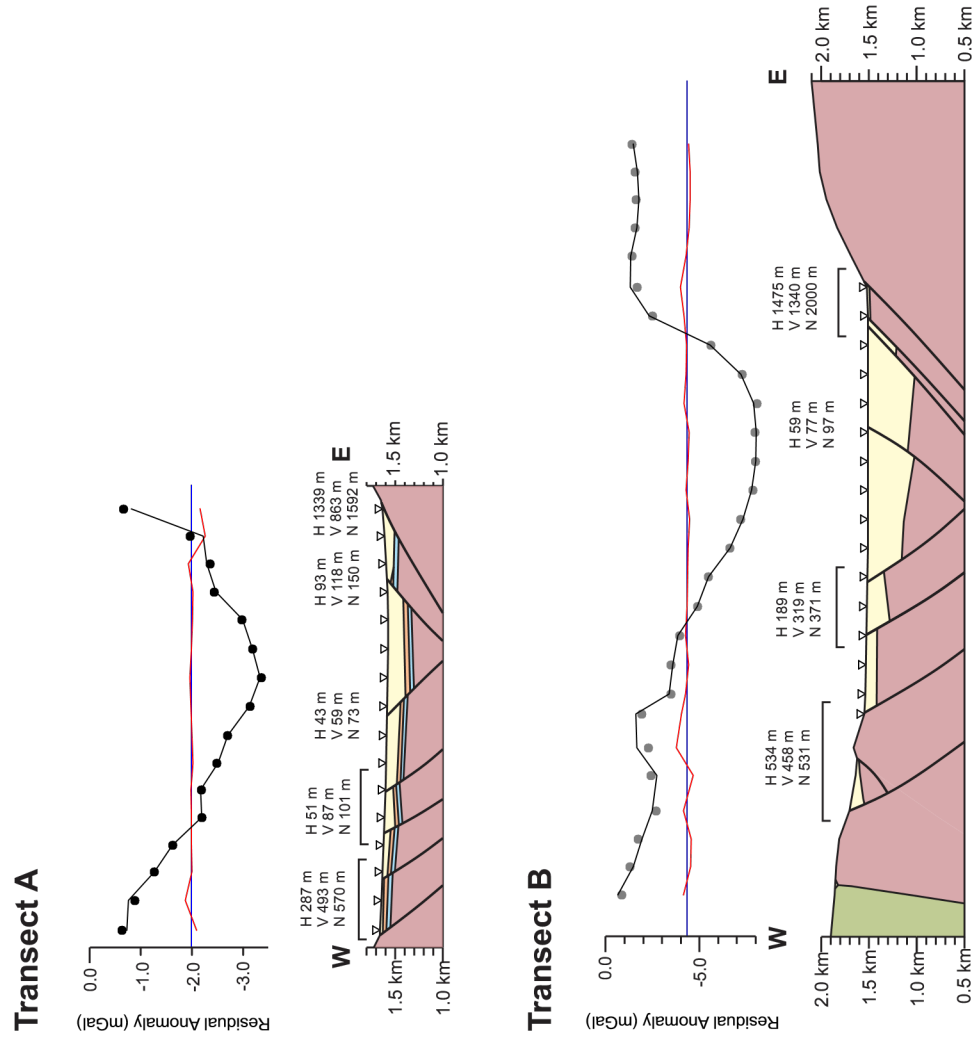


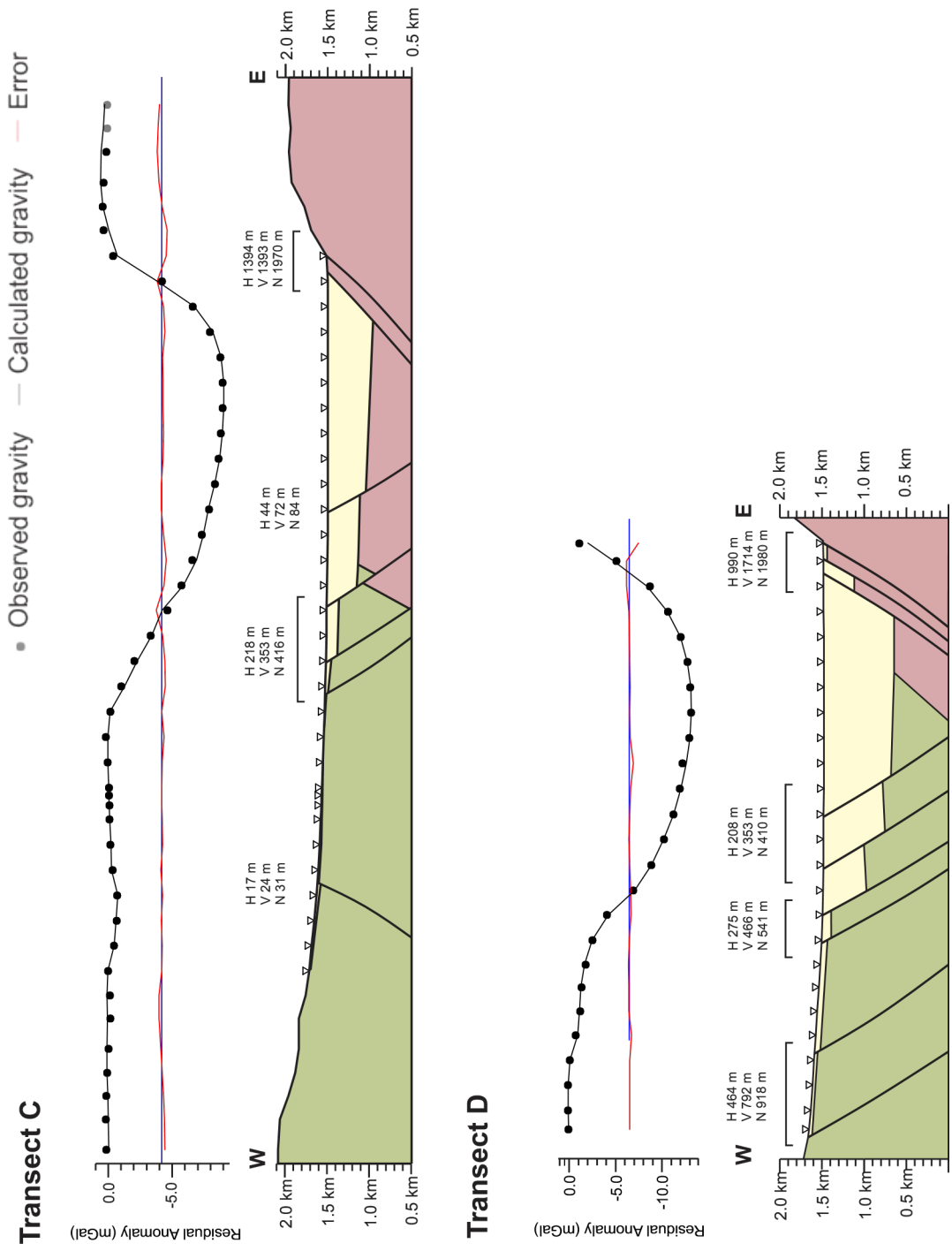
Figure A.8: Geologic map of Deep Springs Valley with two-dimension model transects shown in black. Reference Figure A.3.



• Observed gravity — Calculated gravity — Error



Figures A.9 a-b: Two-dimensional forward models created in GM-SYS Oasis Montaj. Reference Table A.1 for lithology and densities and Figure A.8 for transect locations. Figures A.9 a-d are oriented west-east and are each with in the same scale.



Figures A.9 c-d: Two-dimensional forward models created in GM-SYS Oasis Montaj. Reference Table A.1 for lithology and densities and Figure A.8 for transect locations. Figures A.9 a-d are oriented west-east and are each with in the same scale.

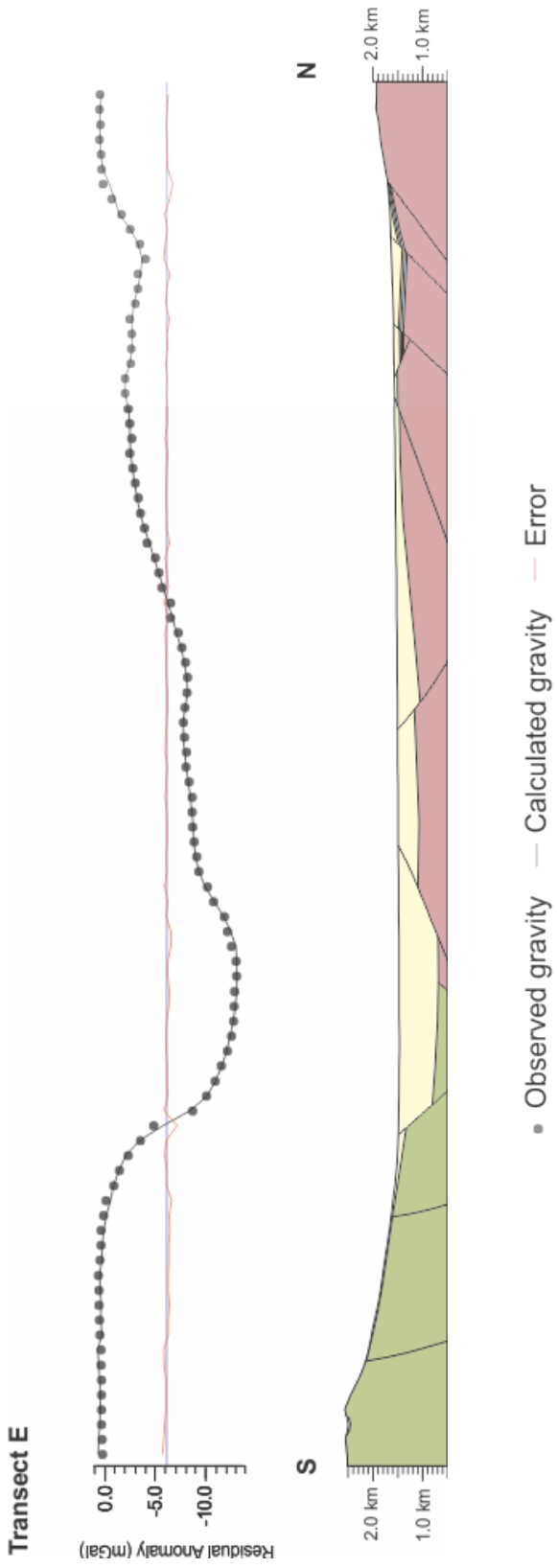


Figure A.9 e: Two-dimensional forward models created in GM-SYS Oasis Montaj. Reference Table A.1 for lithology and densities and Figure A.8 for transect locations. Figure A.9 e is oriented north-northeast to south-south west and has a smaller scale than the previous transects.

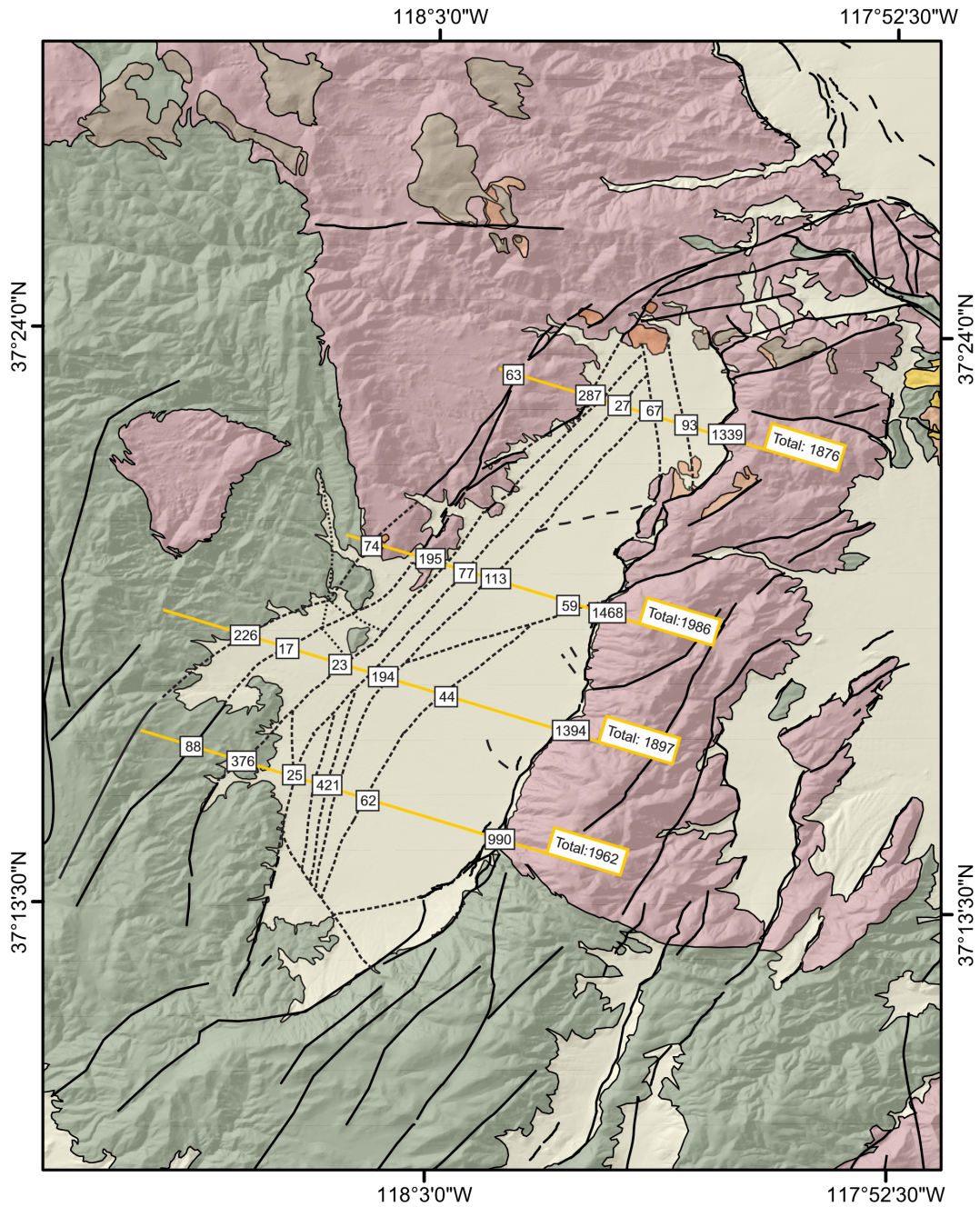


Figure A.10. Geologic map of Deep Springs Valley with displacement budget transects in yellow. Black outlined boxes contain horizontal extension values in meters. Yellow outlined boxes contain total horizontal extension summed along the transect. Fault traces are shown in black solid lines and modelled faults are dashed black lines.

## REFERENCES

- Argus, D.F., and Gordon, R.G., 1991, Current Sierra Nevada-North America motion from very long baseline interferometry: implications for the kinematics of the western United States: *Geology*, v. 19, p. 1085–1088, doi: 10.1130/0091-7613(1991)019<1085:CSNNAM>2.3.CO;2.
- Bennett, R.A., Wernicke, B.P., Niemi, N.A., Friedrich, A.M., and Davis, J.L., 2003, Contemporary strain rates in the northern Basin and Range province from GPS data: *Tectonics*, v. 22, doi: 10.1029/2001TC001355.
- Burchfiel, B.C., Hodges, K. V., and Royden, L.H., 1987, Geology of Panamint Valley - Saline Valley Pull-Apart System, California: Palinspastic Evidence for Low-Angle Geometry of a Neogene Range-Bounding Fault: *Geology*, v. 92, p. 422–426.
- Burchfiel, B.C., and Stewart, J.H., 1966, “pull-apart” origin of the central segment of Death Valley, California: *Bulletin of the Geological Society of America*, v. 77, p. 439–442, doi: 10.1130/0016-7606(1966)77[439:POOTCS]2.0.CO;2.
- Cogbill, A.H., 1990, Gravity terrain corrections calculated using digital elevation models: *Geophysics*, v. 55, p. 102–106.
- Dalrymple, D.B., 1963, Potassium-Argon Dates of Some Cenozoic Volcanic Rocks of the Sierra Nevada, California: *Geological Society of America Bulletin*, v. 74, p. 379–390.
- Dixon, T., Miller, M., Farina, F., Wang, H., and Johnson, D., 2000, Present-day motion of the Sierra Nevada block and some tectonic implications for the Basin and Range province, North American Cordillera: *Tectonics*, v. 19, p. 1–24, doi: 10.1029/1998TC001088.
- Dixon, T.H., Robaudo, S., Lee, J., and Reheis, M.C., 1995, Constraints on present-day Basin and Range deformation from space geodesy: *Tectonics*, v. 14, p. 755–772, doi: 10.1029/95TC00931.
- Dunn, S.B., Oldow, J.S., and Mueller, N.J., 2015, Late Cenozoic displacement transfer in the eastern Sylvania Mountain fault system and Lida Valley pull-apart basin, southwestern Nevada, based on three-dimensional gravity depth inversion and forward models: *Geosphere*, v. 11, p. 1565–1589, doi: 10.1130/GES01151.1.
- Frankel, K. L., 2007a, Cosmogenic  $^{10}\text{Be}$  and  $^{36}\text{Cl}$  geochronology of offset alluvial fans along the northern Death Valley fault zone: Implications for transient strain in the eastern California shear zone: *Journal of Geophysical Research*, v. 112, p. B06407, doi: 10.1029/2006/JB004350.

- Frankel, K. L., Dolan, J. F., Finkel, R. C., Owen, L., and Hoeft, J. S., 2007b, Spatial variations in slip rate along the Death Valley-Fish Lake Valley fault system determined from LiDAR topographic data and cosmogenic <sup>10</sup>Be geochronology: *Geophysical Research Letters*, v. 34, p. L18303, doi: 10.1029/2007/GL030549.
- Frankel, K.L., Dolan, J.F., Owen, L.A., Ganev, P., and Finkel, R.C., 2011, Spatial and temporal constancy of seismic strain release along an evolving segment of the Pacific-North America plate boundary: *Earth and Planetary Science Letters*, v. 304, p. 565–576, doi: 10.1016/j.epsl.2011.02.034.
- Ganev, P.N., Dolan, J.F., Frankel, K.L., and Finkel, R.C., 2010, Rates of extension along the Fish Lake Valley fault and transtensional deformation in the Eastern California shear zone-Walker Lane belt: *Lithosphere*, v. 2, p. 33–49, doi: 10.1130/L51.1.
- Hildenbrand, T.G., Briesacher, A., Flanagan, G., and Hinze, W.J., 2002, Rationale and Operational Plan to Upgrade the U . S Gravity Database: USGS Open File Report, p. 1–12.
- Hinze, W.J., 2003, Bouguer reduction density , why 2 . 67 ? v. 68, p. 1559–1560.
- Hinze, W.J., Aiken, C., Brozena, J., Coakley, B., Dater, D., Flanagan, G., Forsberg, R., Hildenbrand, T., Keller, G.R., Kellogg, J., Kucks, R., Li, X., Mainville, A., Morin, R., et al., 2005, New standards for reducing gravity data: The North American gravity database: *Geophysics*, v. 70, p. J25–J32, doi: 10.1190/1.1988183.
- Kane, M.F., and Pakiser, L.C., 1961, Geophysical Study of Subsurface Structure in Southern Owens Valley, California: *Geophysics*, v. XXVI, p. 12–26.
- Katopody, D.T., 2018, Extensional and Accretionary Tectonics of Western North America: Examples from the Southern Walker Lane and Northwestern Washington State: The University of Texas at Dallas.
- Kirby, E., Anandakrishnan, S., Phillips, F., and Marrero, S., 2008, Late Pleistocene slip rate along the Owens Valley fault, eastern California: *Geophysical Research Letters*, v. 35, p. 2–7, doi: 10.1029/2007GL031970.
- Lee, J., Rubin, C.M., and Calvert, A., 2001, Quaternary faulting history along the Deep Springs fault, California: *Bulletin of the Geological Society of America*, v. 113, p. 855–869, doi: 10.1130/0016-7606(2001)113<0855:QFHATD>2.0.CO;2.
- Mckee, E. H. and Nelson, C. A., 1967, Geologic map of the Soldier Pass Quadrangle, California and Nevada: U. S. Geological Survey, Report: GQ-0654, scale 1:62,500.
- Mckee, E.H., 1968, Age and Rate of Movement of the Northern Part of the Death Valley-Furnace Creek Fault Zone, California: *GSA Bulletin*, v. 79, p. 1–18, doi: 10.1130/0016-7606(1968)79.

- Miller, W.J., 1928, Geology of Deep Spring Valley , California: *The Journal of Geology*, v. 36, p. 510–525, <https://www.jstor.org/stable/30059947>.
- Mueller, N. J. and Oldow, J.S., 2018, Pliocene to Holocene Displacement Budget Along the Fish Lake Valley Fault Zone, Eastern California - Southwestern Nevada: *American Association of Petroleum Geologists*, v. , p. .
- Nelson, C. A., 1966, Geologic map of the Blanco Mountain Quadrangle, Inyo and Mono counties, California: U. S. Geological Survey, Report: GQ-0529, scale 1:62,500.
- Nelson, C. A., 1971, Geologic map of the Waucoba Spring Quadrangle, Inyo County, California: U. S. Geological Survey, Report: GQ-0921, scale 1:62,500.
- Nelson, C. A., 1966, Geologic map of the Waucoba Mountain Quadrangle, Inyo County, California: U. S. Geological Survey, Report: GQ-0528, scale 1:62,500.
- Nelson, C.A., 1978, Late Precambrian–Early Cambrian stratigraphic and faunal succession of eastern California and the Precambrian–Cambrian boundary: *Geological Magazine*, v. 115, p. 121, doi: 10.1017/S0016756800041169.
- Oldow, J.S., 2003, Active transtensional boundary zone between the western Great Basin and Sierra Nevada block, western U.S. Cordillera: *Geology*, v. 31, p. 1033–1036, doi: 10.1130/G19838.1.
- Oldow, J.S., 1992, Late Cenozoic displacement partitioning in the northwestern Great Basin.: Structure, Tectonics and Mineralization of the Walker Lane, Stewart, J., ed., Walker Lane Symposium Proceedings Volume, Geological Society of Nevada, Reno, NV, p. 17–52.
- Oldow, J.S., Aiken, C.L. V, Hare, J.L., Ferguson, J.F., and Hardyman, R.F., 2001, Active displacement transfer and differential block motion within the central Walker Lane, western Great Basin: *Geology*, v. 29, p. 19–22, doi: 10.1130/0091-7613(2001)029<0019.
- Oldow, J.S., Geissman, J.W., and Stockli, D.F., 2008, Evolution and Strain Reorganization within Late Neogene Structural Stepovers Linking the Central Walker Lane and Northern Eastern California Shear Zone, Western Great Basin: *International Geology Review*, v. 50, p. 270–290, doi: 10.2747/0020-6814.50.3.270.
- Pakiser, L.C., Kane, M.F., and Jackson, W.H., 1964, Structural Geology and Volcanism of Owens Valley Region, California-A Geophysical Study: U.S. Geological Survey Professional Paper 438, p. 73.
- Pan American Center for Earth and Environmental Studies (PACES), 2005, The University of Texas at El Paso, Gravity database of the United States: <http://www.research.utep.edu>.

- Reheis, M.C., and Dixon, T.H., 1996, Kinematics of the Eastern California shear zone: Evidence for slip transfer from Owens and Saline Valley fault zones to Fish Lake Valley fault zone: *Geology*, v. 24, p. 339–342, doi: 10.1130/0091-7613(1996)024<0339:KOTECS>2.3.CO;2.
- Reheis, M.C., and Sawyer, T.L., 1997, Late Cenozoic history and slip rates of the Fish Lake Valley, Emigrant Peak, and Deep Springs fault zones, Nevada and California: *Bulletin of the Geological Society of America*, v. 109, p. 280–299, doi: 10.1130/0016-7606(1997)109<0280:LCHASR>2.3.CO;2.
- Renik, B., and Christie-Blick, N., 2015, A new hypothesis for the amount and distribution of dextral displacement along the Fish Lake Valley-northern Death Valley-Furnace Creek fault zone, California-Nevada: *Tectonics*, v. 32, p. 123–145, doi: 10.1029/2012TC003170.
- Stewart, J., 1988, Tectonics of the Walker Lane Belt, Western Great Basin: Mesozoic and Cenozoic Deformation in a zone of Shear: *Rubey*, v. 7, p. 683–713.
- Wilson, D.V., 1975, Geophysical investigation of the sub- surface structure of Deep Springs Valley, California [Master's thesis]: Los Angeles, University of California, 65 p.



## **BIOGRAPHICAL SKETCH**

Sarah Sokol was born in Dallas, Texas in 1991. She attended Richardson ISD schools until her graduation from Richardson High School in 2009. Sarah received her Bachelor of Science in Geosciences at The University of Texas at Dallas in May 2017. She began graduate level courses, as a part of the graduate fast-track program, in August 2016 at The University of Texas at Dallas. Sarah completed her Master of Science in Geosciences in the spring of 2019.

## **CURRICULUM VITAE**

**Sarah A. Sokol**

800 W. Campbell Rd, Richardson, TX 75080

Sas096020@utdallas.edu

### **Education**

#### **Bachelor of Science in Geosciences**

The University of Texas at Dallas

Graduated May 2017

#### **Master of Science in Geosciences**

The University of Texas at Dallas

Graduation May 2019

### **Awards and Accomplishments**

University of Texas at Dallas Dean's List, Spring and Fall 2016

Pioneer Natural Resources Scholarship, Fall 2016 through Fall 2019